UNIWERSYTET WARSZAWSKI

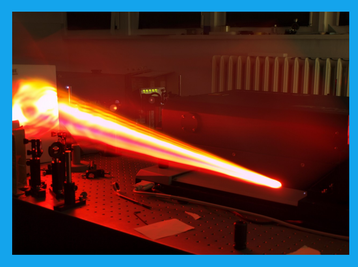

In Femto Research Group

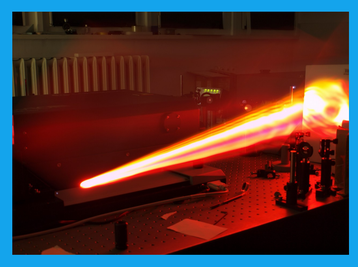

WCh Wydział Chemii Uniwersytet Warszawski

Chemical Science

PICK OF THE WEEK

ROYAL SOCIETY OF CHEMISTRY

EDGE ARTICLE

View Article Online
View Journal | View Issue

Check for updates

Cite this: *Chem. Sci.*, 2021, **12**, 14039

All publication charges for this article have been paid for by the Royal Society of Chemistry

Potent strategy towards strongly emissive nitroaromatics through a weakly electron-deficient core†

Bartłomiej Sadowski,‡[a] Marzena Kaliszewska,[b] Yevgen M. Poronik,[a] Małgorzata Czichy,[c] Patryk Janasik,[c] Marzena Banasiewicz,[d] Dominik Mierzwa,[a] Wojciech Gadomski,[b] Trevor D. Lohrey,[ef] John A. Clark,[g] Mieczysław Łapkowski,*[c] Bolesław Kozankiewicz,*[d] Valentine I. Vullev,*[ghij] Andrzej L. Sobolewski,*[d] Piotr Piatkowski*[b] and Daniel T. Gryko*[a]

Nitroaromatics seldom fluoresce. The importance of electron-deficient (n-type) conjugates, however, has inspired a number of strategies for suppressing the emission-quenching effects of the strongly electron-withdrawing nitro group. Here, we demonstrate how such strategies yield fluorescent nitroaryl derivatives of dipyrrolonaphthyridinedione (DPND). Nitro groups near the DPND core quench its fluorescence. Conversely, nitro groups placed farther from the core allow some of the highest fluorescence quantum yields ever recorded for nitroaromatics. This strategy of preventing the known processes that compete with photoemission, however, leads to the emergence of unprecedented alternative mechanisms for fluorescence quenching, involving transitions to dark nπ* singlet states and aborted photochemistry. Forming nπ* triplet states from ππ* singlets is a classical pathway for fluorescence quenching. In nitro-DPNDs, however, these ππ* and nπ* excited states are both singlets, and they are common for nitroaryl conjugates. Understanding the excited-state dynamics of such nitroaromatics is crucial for designing strongly fluorescent electron-deficient conjugates.

Received 6th July 2021
Accepted 5th September 2021

DOI: 10.1039/d1sc03670j

rsc.li/chemical-science

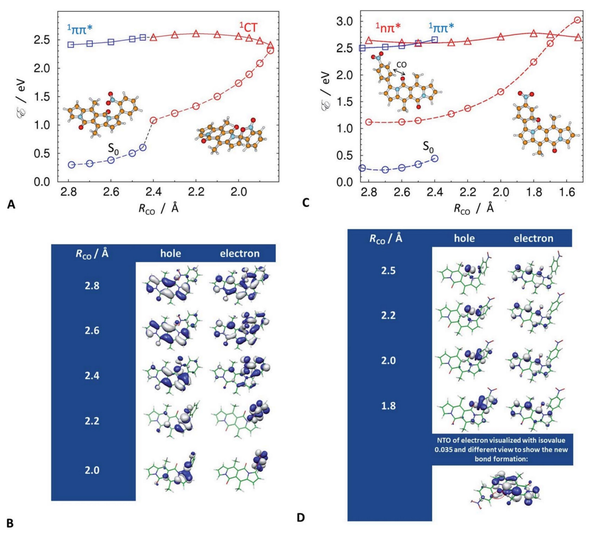

Fig. 9 Potential-energy profiles (PEPs) along the carbon–oxygen distances, R_{CO}, and the corresponding $S_1 \rightarrow S_0$ NTOs (isovalues = 0.03, unless indicated otherwise) optimized with the ADC(2)/def-SV(P) method in the lowest excited singlet states of (A and B) **5** and (C and D) **3**. (A and C) Circles connected by dashed line denote vertical energy of the ground state computed at the geometry of the respective excited state. For **5**, (A) locally-excited, $^1\pi\pi^*$, state – blue squares, and the dark charge-transfer, ^{1}CT, state – red triangles; and (B) NTOs along R_{CO}. For **3**, (C) locally-excited, $^1\pi\pi^*$, state – blue squares, and the dark $^1n\pi^*$ state – red triangles; and (D) NTOs along R_{CO}, where the last bottom structure depicts the electron NTO at isovalue of 0.035 to visualize the formation of the carbon–oxygen covalent bond, as circled with a red dashed line.

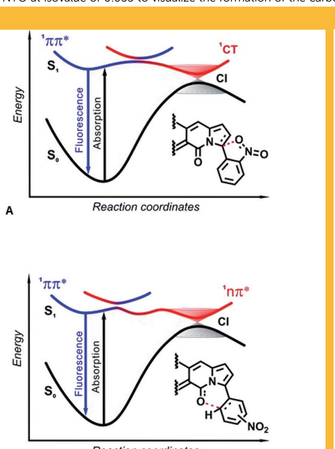

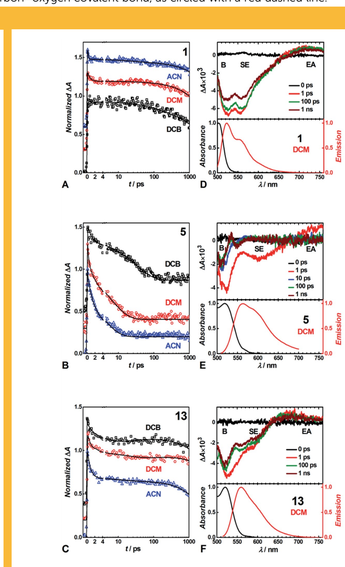

Fig. 6 Transient absorption decays normalized to 1 of (A) **1**, (B) **5** and (C) **13** in different solvents at observation wavelength of 520 nm. Transient absorption spectra at different pump-probe time delays (upper panel) and time-integrated absorption and emission spectra normalized to 1 (lower panel) of (D) **1**, (E) **5** and (F) **13** in DCM. The transient absorption signals were recorded upon excitation at 480 nm. Solid lines are from global multiexponential fits to the experimental data. For clarity the transient absorption decays were offset on the *y*-axis. B – bleach band, SE – stimulated emission, EA – excited state absorption.

Członkowie zespołu

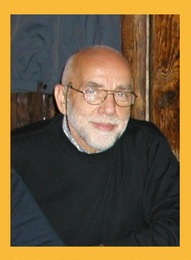

prof. dr hab. Wojciech Gadomski (kierownik grupy)

dr hab. Bożena Ratajska-Gadomska

dr Kamil Polok

dr Piotr Piątkowski

Karolina Skała

Adam Świątek

Marzena Kaliszewska

THE JOURNAL OF PHYSICAL CHEMISTRY C
A JOURNAL OF THE AMERICAN CHEMICAL SOCIETY

pubs.acs.org/JPCC

Article

Effect of the Mixture Composition of $BmimBF_4$–Acetonitrile on the Excited-State Relaxation Dynamics of a Solar-Cell Dye D149: An Ultrafast Transient Absorption Study

Nishith Maity, Piotr Piatkowski,* Kamil Polok,* François-Alexandre Miannay, and Abdenacer Idrissi*

Cite This: *J. Phys. Chem. C* 2021, 125, 17841–17852

Read Online

ACCESS | Metrics & More | Article Recommendations | Supporting Information

ABSTRACT: The excited-state relaxation dynamics of D149, one of the metal-free substituted indoline dyes used in dye-sensitized solar cells, is studied in the whole composition range of the 1-butyl-3-methylimidazolium tetrafluoroborate ($BmimBF_4$)–acetonitrile binary mixture by using time-integrated absorption, emission, and time-resolved transient absorption (TA) spectroscopies. The comparative analysis of absorption and emission spectra indicates that the value of Stokes shift reduces monotonically with decreasing mixture polarity. The global analysis of time-resolved TA spectra indicates the presence of four different time components related to different processes in the excited state of the dye. Importantly, the observed timescales are highly sensitive to composition, polarity, and viscosity of the binary mixture. Increase of viscosity and decrease of polarity observed for increasing ionic liquid (IL) content in the mixture lead to overall increase in the emission lifetime (S_1–S_0) of D149. At a lower IL mole fraction (X_{IL} = 0.1), the emission lifetime shows a minimum that can be traced back to the change from the situation in which the local environment of the dye is dominated by the interactions in acetonitrile to that in which it is dominated by those in $BmimBF_4$. This also is reflected in the occurrence of a minimum in relative quantum yield in the same range of X_{IL}. The origin of the other moderately long-time component (33 ps in ACN-120 ps in $BmimBF_4$) is still debatable; however, for pure IL and all the mixtures, the composition dependence of this timescale is similar to that of the longest emission lifetime.

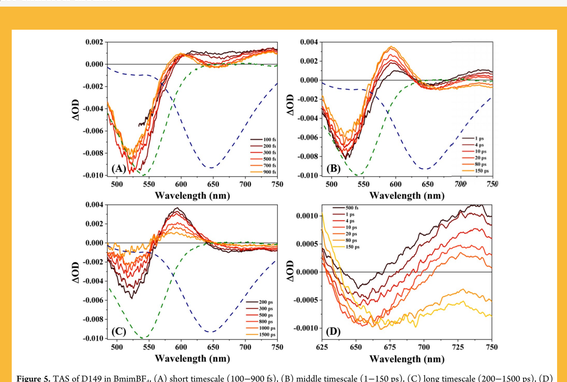

Figure 5. TAS of D149 in $BmimBF_4$ (A) short timescale (100−900 fs), (B) middle timescale (1−150 ps), (C) long timescale (200−1500 ps), (D) solvation timescale. Dashed spectra are steady-state absorption (green) and emission (blue) spectra.

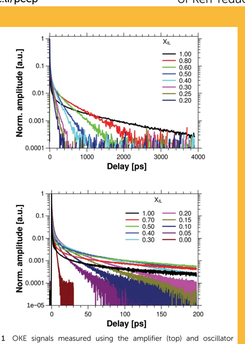

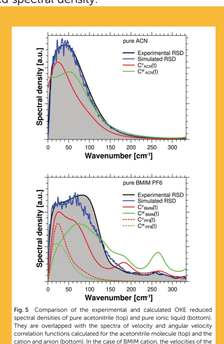

Fig. 1 OKE signals measured using the amplifier (top) and oscillator (bottom) setups.

Fig. 5 Comparison of the experimental and calculated OKE reduced spectral densities of pure acetonitrile (top) and pure ionic liquid (bottom). They are overlapped with the spectra of velocity and angular velocity correlation functions calculated for the acetonitrile molecule (top) and the cation and anion (bottom). In the case of BMIM cation, the velocities of the centre of mass of the imidazolium ring are used.

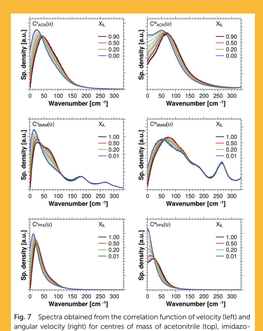

Fig. 7 Spectra obtained from the correlation function of velocity (left) and angular velocity (right) for centres of mass of acetonitrile (top), imidazolium ring of BMIM cation (middle) and the PF_6 anion (bottom).

PCCP

ROYAL SOCIETY OF CHEMISTRY

PAPER

View Article Online
View Journal | View Issue

Check for updates

Cite this: *Phys. Chem. Chem. Phys.*, 2020, **22**, 24544

Dynamics in the BMIM PF_6/acetonitrile mixtures observed by femtosecond optical Kerr effect and molecular dynamics simulations†

Kamil Polok,*[a] Matthieu Beisert,[b] Adam Świątek,[a] Nishith Maity,[b] Piotr Piatkowski,[d] Wojciech Gadomski,[c] François Alexandre Miannay[b] and Abdenacer Idrissi*[b]

We have performed the measurements of the optical Kerr effect signal time evolution up to 4 ns for a mixture of 1-alkyl-3-methyl-imidazolium hexafluorophosphate (BMIM PF_6) ionic liquid and acetonitrile in the whole mole fractions range. The long delay line in our experimental setup allowed us to capture the complete reorientational dynamics of the ionic liquid. We have analysed the optical Kerr effect signal in the time and frequency domains with help of molecular dynamics simulations. In our approximation of the slow picosecond dynamics with a multi-exponential decay, we distinguish three relaxation times. The highest two are assigned to the reorientation of the cation and acetonitrile molecules that are in the vicinity of the imidazolium ring. The third one is recognized as originating from cation rotations and reorientation of acetonitrile molecules in the bulk or in the vicinity of the aliphatic chains of the cation. With help of the simulation we interpret the intermolecular band in the reduced spectral density, obtained from Kerr signal, as follows: its low-frequency side results from oscillations of one of the components in the cage formed by its neighbors, while the high-frequency side is attributed to the librations of the cation and acetonitrile molecule as well as the intermolecular oscillations of system components involved in specific interactions. We use this assignment and concentration dependence of the spectra obtained from velocity and angular velocity correlations to explain the mole fraction dependence of Kerr reduced spectral density.

Received 20th July 2020,
Accepted 14th October 2020

DOI: 10.1039/d0cp03847d

rsc.li/pccp

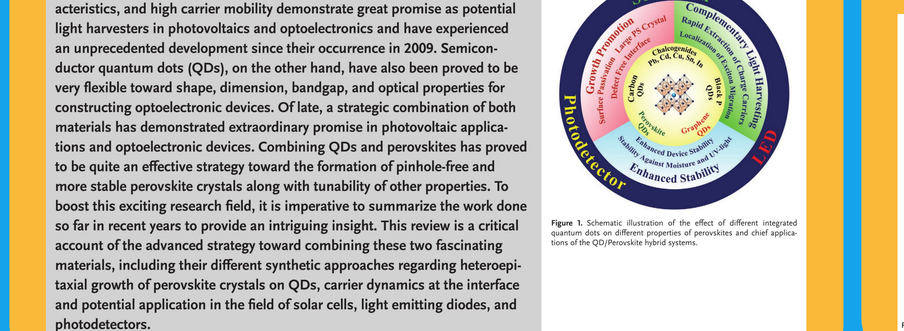

REVIEW

ADVANCED OPTICAL MATERIALS
www.advopticalmat.de

Combining Perovskites and Quantum Dots: Synthesis, Characterization, and Applications in Solar Cells, LEDs, and Photodetectors

*Soumyadipta Rakshit, Piotr Piatkowski, Iván Mora-Seró, and Abderrazzak Douhal**

Metal halide perovskites having high defect tolerance, high absorption characteristics, and high carrier mobility demonstrate great promise as potential light harvesters in photovoltaics and optoelectronics and have experienced an unprecedented development since their occurrence in 2009. Semiconductor quantum dots (QDs), on the other hand, have also been proved to be very flexible toward shape, dimension, bandgap, and optical properties for constructing optoelectronic devices. Of late, a strategic combination of both materials has demonstrated extraordinary promise in photovoltaic applications and optoelectronic devices. Combining QDs and perovskites has proved to be quite an effective strategy toward the formation of pinhole-free and more stable perovskite crystals along with tunability of other properties. To boost this exciting research field, it is imperative to summarize the work done so far in recent years to provide an intriguing insight. This review is a critical account of the advanced strategy toward combining these two fascinating materials, including their different synthetic approaches regarding heteroepitaxial growth of perovskite crystals on QDs, carrier dynamics at the interface and potential application in the field of solar cells, light emitting diodes, and photodetectors.

Figure 1. Schematic illustration of the effect of different integrated quantum dots on different properties of perovskites and chief applications of the QD/Perovskite hybrid systems.

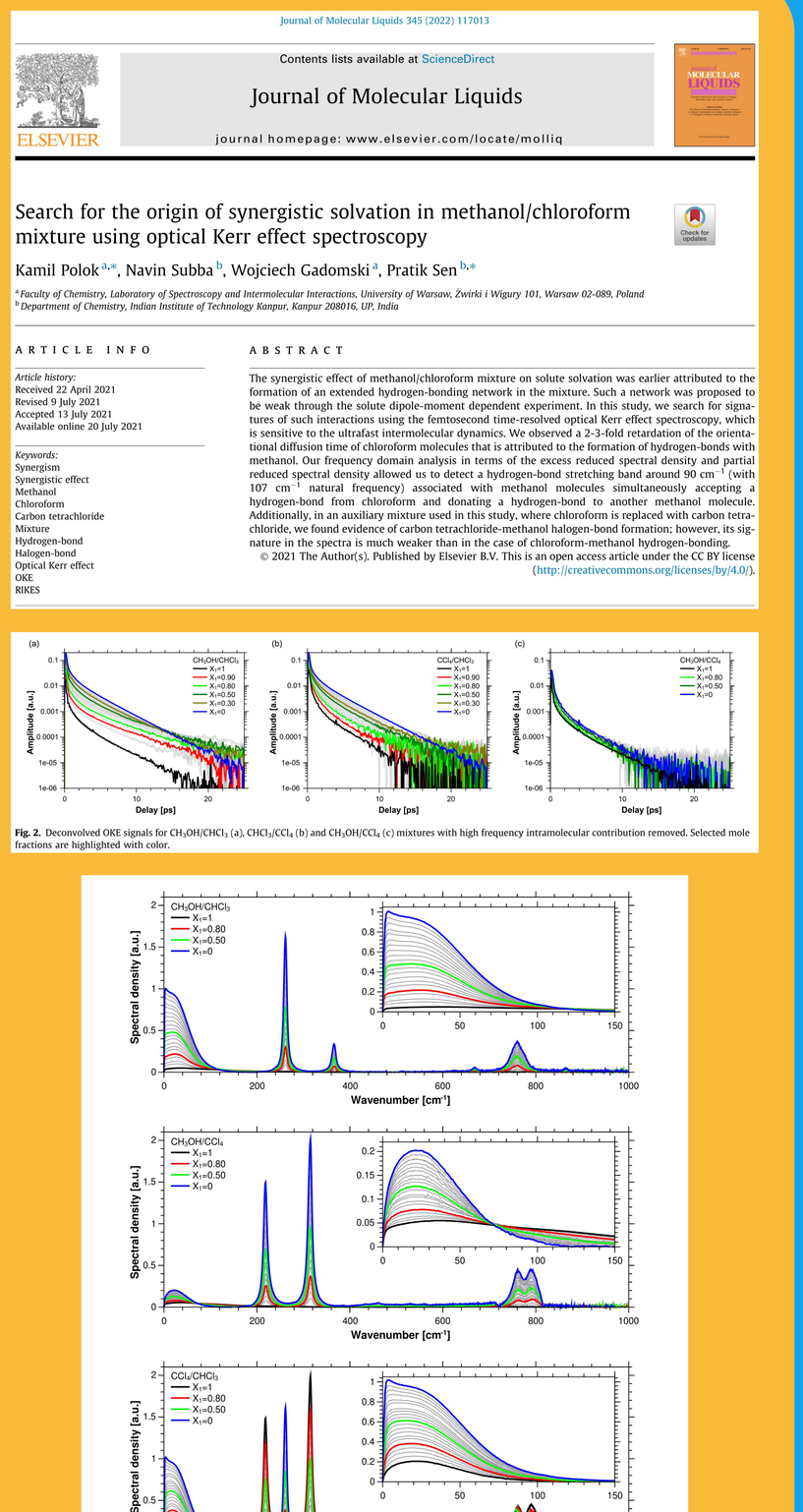

Figure S22: Mole fraction dependence of the OKE total spectral density for $CH_3OH/CHCl_3$, CH_3OH/CCl_4 and $CCl_4/CHCl_3$ mixtures. The insets show the intermolecular band in the 0-150 cm^{-1} range.

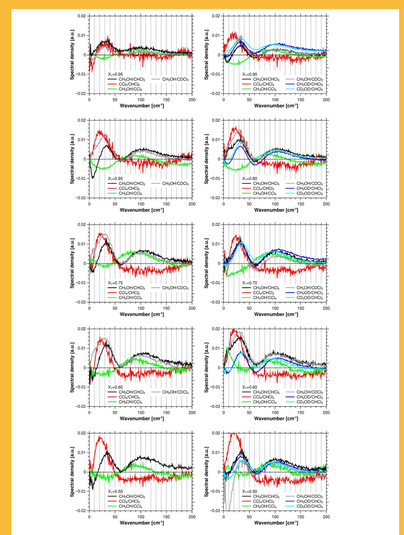

Figure S28: Comparison of the ERSDs for the investigated systems at all considered mole fractions. The excess spectra are background corrected with $S_{bg} = A\omega$ function, where A is set so that the average value in the 400–450 cm^{-1} range is zero.

Figure S28: (cont.) Comparison of the ERSDs for the investigated systems at all considered mole fractions.

Journal of Molecular Liquids 345 (2022) 117013

Contents lists available at ScienceDirect

Journal of Molecular Liquids

journal homepage: www.elsevier.com/locate/molliq

Search for the origin of synergistic solvation in methanol/chloroform mixture using optical Kerr effect spectroscopy

Kamil Polok [a,*], Navin Subba [b], Wojciech Gadomski [a], Pratik Sen [b,*]

[a] Faculty of Chemistry, Laboratory of Spectroscopy and Intermolecular Interactions, University of Warsaw, Żwirki i Wigury 101, Warsaw 02-089, Poland
[b] Department of Chemistry, Indian Institute of Technology Kanpur, Kanpur 208016, UP, India

ARTICLE INFO

Article history:
Received 22 April 2021
Revised 9 July 2021
Accepted 13 July 2021
Available online 20 July 2021

Keywords:
Synergism
Synergistic effect
Methanol
Chloroform
Carbon tetrachloride
Mixture
Hydrogen-bond
Halogen-bond
Optical Kerr effect
OKE
RIKES

ABSTRACT

The synergistic effect of methanol/chloroform mixture on solute solvation was earlier attributed to the formation of an extended hydrogen-bonding network in the mixture. Such a network was proposed to be weak through the solute dipole-moment dependent experiment. In this study, we search for signatures of such interactions using the femtosecond time-resolved optical Kerr effect spectroscopy, which is sensitive to the ultrafast intermolecular dynamics. We observed a 2-3-fold retardation of the orientational diffusion time of chloroform molecules that is attributed to the formation of hydrogen-bonds with methanol. Our frequency domain analysis in terms of the excess reduced spectral density and partial reduced spectral density allowed us to detect a hydrogen-bond stretching band around 90 cm^{-1} (with 107 cm^{-1} natural frequency) associated with methanol molecules simultaneously accepting a hydrogen-bond from chloroform and donating a hydrogen-bond to another methanol molecule. Additionally, in an auxiliary mixture used in this study, where chloroform is replaced with carbon tetrachloride, we found evidence of carbon tetrachloride-methanol halogen-bond formation; however, its signature in the spectra is much weaker than in the case of chloroform-methanol hydrogen-bonding.

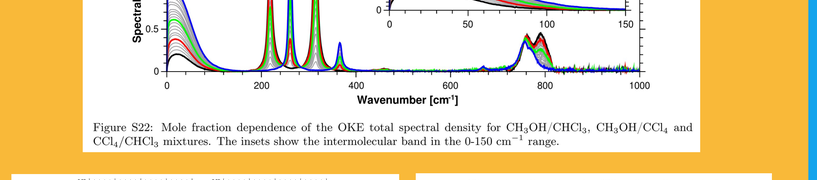

Fig. 2. Deconvolved OKE signals for $CH_3OH/CHCl_3$ (a), $CHCl_3/CCl_4$ (b) and CH_3OH/CCl_4 (c) mixtures with high frequency intramolecular contribution removed. Selected mole fractions are highlighted with color.

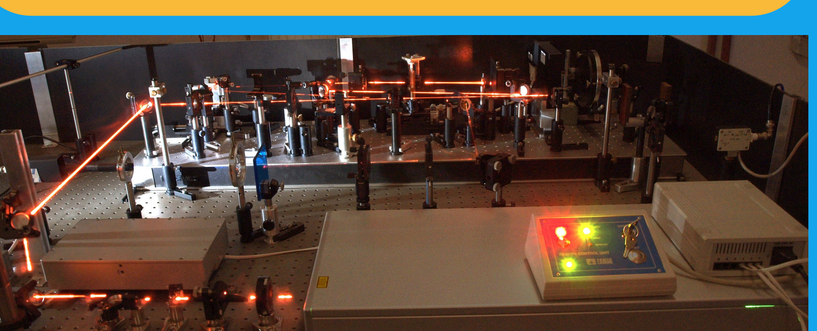

Figure S22: Mole fraction dependence of the OKE total spectral density for $CH_3OH/CHCl_3$, CH_3OH/CCl_4 and $CCl_4/CHCl_3$ mixtures. The insets show the intermolecular band in the 0-150 cm^{-1} range.

Figure S28: Comparison of the ERSDs for the investigated systems at all considered mole fractions. The excess spectra are background corrected with $S_{bg} = A\omega$ function, where A is set so that the average value in the 400–450 cm^{-1} range is zero.

Figure S28: (cont.) Comparison of the ERSDs for the investigated systems at all considered mole fractions.